

Supplementary Information

Target-induced photocurrent-polarity switching: highly selective and sensitive photoelectrochemical sensing platform

Ruiying Yang, Kang Zou, Xiaohua Zhang, Cuicui Du, Jinhua Chen*

State Key Laboratory of Chemo/Biosensing and Chemometrics, College of Chemistry and Chemical Engineering, Hunan University, Changsha, 410082, P. R. China

List of Contents:

- 1. Materials and reagents**
- 2. Apparatus**
- 3. Synthesis of NPC-ZnO/Au/CdS polyhedra**
- 4. Fabrication of the PEC biosensor and PEC assay**
- 5. TEM images of NPC-ZnO and NPC-ZnO/Au polyhedra**
- 6. EDS spectrum of NPC-ZnO/Au polyhedra**
- 7. EDS spectrum of NPC-ZnO/Au/CdS polyhedra**
- 8. EDS mapping images of NPC-ZnO/Au/CdS polyhedra**
- 9. XRD pattern of NPC-ZnO/Au/CdS polyhedra**
- 10. XPS spectrum of NPC-ZnO/Au/CdS polyhedra**
- 11. The schematic illustration of the structure of this NPC-ZnO/Au/CdS polyhedra**

* Corresponding author. Tel.: +86-731-88821848

E-mail address: chenjinhua@hnu.edu.cn

- 12. The possible electron-transfer mechanism of ITO/NPC-ZnO/Au and ITO/NPC-ZnO/Au/CdS electrodes**
- 13. Hemin-induced photocurrent-polarity switching**
- 14. Optimization of experimental conditions**
- 15. Comparison of various PEC methods for TB assay**
- 16. Selectivity, reproducibility and stability**
- 17. Recovery test**
- 18. References**

1. Materials and reagents

6-mercaptohexanol (MCH), tris-(2-carboxyethyl) phosphine hydrochloride (TCEP), human α -thrombin (TB), and chloroauric acid ($\text{HAuCl}_4 \cdot 4\text{H}_2\text{O}$) were purchased from Sigma-Aldrich (USA). The ITO slices were provided by Zhuhai Kaivo Electronic Components Co., Ltd, China. Sodium borohydride (NaBH_4), cadmium nitrate ($\text{Cd}(\text{NO}_3)_2 \cdot 4\text{H}_2\text{O}$), L-cysteine, zinc nitrate hexahydrate ($\text{Zn}(\text{NO}_3)_2 \cdot 6\text{H}_2\text{O}$), 2-methylimidazole (2-MI), ascorbic acid (AA), and ethanol were all provided by Sinopharm Chemical Reagent Co., Ltd. (China). All of the other reagents were analytical grade. Oligonucleotides were supplied by Sangon Biotechnology Co. Ltd. (Shanghai, China), and the related sequences are as follows: TBA1: 5'-SH-(CH_2)₆-CCA ACC ACA CCA ACC-3'. TBA2: 5'-GGT TGG TGT GGT TGG AGA AGA AGG TGT TTA AGT A-3'. HP1: 5'-AGG GCG GGT GGG TGT TTA AGT TGG AGA ATT GTA CTT AAA CAC CTT CTT CTT GGG T-3'. HP2: 5'-TGG GTC AAT TCT CCA ACT TAA ACT AGA AGA AGG TGT TTA AGT TGG GTA GGG CGG G-3'. Ultrapure H_2O used in all solutions was purified by a Milli-Q purification system (Millipore Corp., Bedford, MA).

2. Apparatus

The morphology the synthesized materials was characterized by transmission electron microscopy (TEM, JEM-2100F, Japan). The X-ray photoelectron spectroscopy (XPS) was carried out an ESCALAB 250 spectrometer (Thermo-VG Scientific Co. USA). The UV-vis spectra were obtained using a UV-2500 UV-vis spectrophotometer (LabTech). X-ray diffraction (XRD) experiments were performed

through the X-ray diffractometer (PXRD, D/MAX-RA, Japan). A xenon lamp of 300W (PLS-SXE) equipped with a 420 nm filter was acted as the excitation source to provide visible light with > 420 nm because the ultraviolet (UV) light may inevitably cause the damage of biomolecules. PEC and Electrochemical impedance spectroscopy (EIS) tests were performed on a CHI 660D electrochemical working station with a three-electrode system: a modified ITO electrode (a geometrical area of 0.246 cm^2) as the working electrode, a platinum wire as the counter electrode, and a saturated calomel electrode (SCE) as the reference electrode.

3. Synthesis of NPC-ZnO/Au/CdS polyhedra

ZIF-8-derived nitrogen doped porous carbon-ZnO (NPC-ZnO) polyhedra were synthesized according to the previous paper [1]. To prepare NPC-ZnO/Au/CdS polyhedra, NPC-ZnO polyhedra (5 mg) were dispersed in 20 ml ultrapure water by sonicating. Then, the NPC-ZnO polyhedra solution was incubated with the $40 \mu\text{L}$ of 20 wt% HAuCl_4 solution for 30 min. Subsequently, the 5 mL of 20 mM NaBH_4 solution was added into the above solution under stirring for 20 min. HAuCl_4 was reduced by NaBH_4 and Au NPs were formed on the surface of the NPC-ZnO polyhedra. The NPC-ZnO/Au polyhedra were obtained and collected by centrifugation and washing. Subsequently, the 200 mg NPC-ZnO/Au polyhedra was dispersed into 10 mL L-cysteine aqueous solution (0.04 M) containing $\text{Cd}(\text{NO}_3)_2$ (0.2 mmol) and stirred for 2 h to achieve the adsorption of L-cysteine on the surface of Au NPs. Then, 70 mL ethanol was introduced into the resulting suspension. After that, the suspension was subsequently transferred to a 100 mL Teflon-lined autoclave and

heated at 160 °C for 4 h. The final products (NPC-ZnO/Au/CdS polyhedra) were collected and washed with ultrapure water, and then the as-prepared sample was dried at 60 °C.

4. Fabrication of the PEC biosensor and PEC assay

Before use, ITO electrodes were sequentially ultrasonically treated with acetone, 1 M NaOH in ethanol/water mixture (v/v, 1:1), and H₂O. Subsequently, 25 μL NPC-ZnO/Au/CdS polyhedra suspension were dropped onto the cleaned ITO electrode surface and dried, the obtained electrode was labeled as ITO/NPC-ZnO/Au/CdS electrode. Before immobilized on the surface of the obtained electrode, the TBA1 was dissolved in Tris-HCl solution (20 mM, pH 7.4, 140 mM NaCl, 1 mM MgCl₂, 5 mM KCl, 1 mM CaCl₂ and 10 mM TCEP), and incubated for 1 h to decrease disulfide bonds. Then, 20 μL TBA1 solution (1 μM) was coated onto the ITO/NPC-ZnO/Au/CdS electrode surface at 4 °C for 16 h. After that, the obtained ITO/NPC-ZnO/Au/CdS/TBA1 electrode was immersed into 2 mM MCH for 1 h to prevent the non-specific adsorption. Next, the obtained modified electrode was incubated with 20 μL Tris-HCl solution (20 mM, PH 7.4, 140 mM NaCl, 1 mM CaCl₂, 5 mM KCl and 1 mM MgCl₂) containing different-concentration TB at room temperature for 60 min to get ITO/NPC-ZnO/Au/CdS/TBA1/MCH/TB electrode. Then, 20 μL of TBA2 solution (1.5 μM) was coated on the modified electrode surface at room temperature for 1 h.

Before HCR reaction, HP1 and HP2 were separately annealed at 95 °C for 5 min and naturally cooled to room temperature. Then, the mixture of HP1 (1.5 μM), HP2

(1.5 μM) and hemin (0.25 mM) were incubated for 90 min at 37 $^{\circ}\text{C}$ to form the HCR reaction. Then, the mixture solutions were transferred into the modified electrode surface and incubated for 1 h to obtain the ITO/NPC-ZnO/Au/CdS/TBA1/MCH/TB/TBA2/HP1+HP2+hemin electrode. Finally, the PEC investigates were performed in Tris–HCl solution (0.1 M, pH 7.4) containing AA (0.1 M) at -0.3 V.

5. TEM images of NPC-ZnO and NPC-ZnO/Au polyhedra

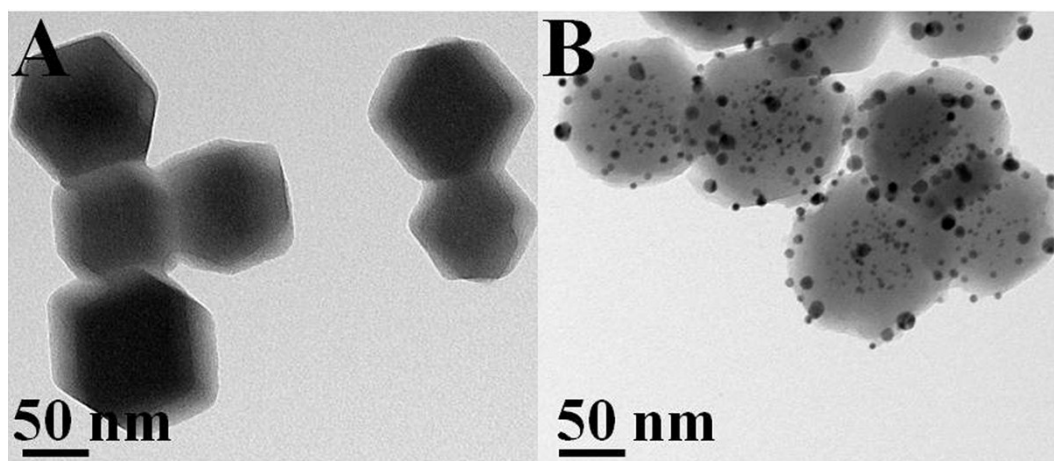


Fig. S1 TEM images of (A) NPC-ZnO and (B) NPC-ZnO/Au polyhedra.

6. EDS spectrum of NPC-ZnO/Au polyhedra

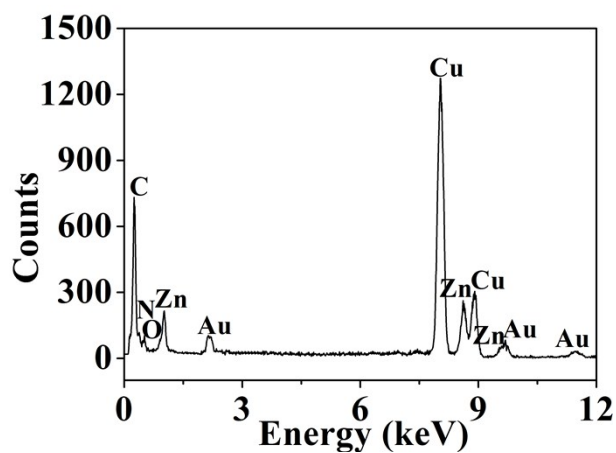


Fig. S2 EDS spectrum of NPC-ZnO/Au polyhedra.

7. EDS spectrum of NPC-ZnO/Au/CdS polyhedra

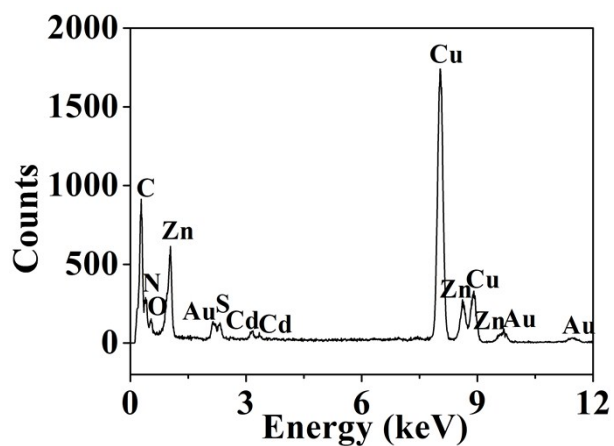


Fig. S3 EDS spectrum of NPC-ZnO/Au/CdS polyhedra.

8. EDS mapping images of NPC-ZnO/Au/CdS polyhedra

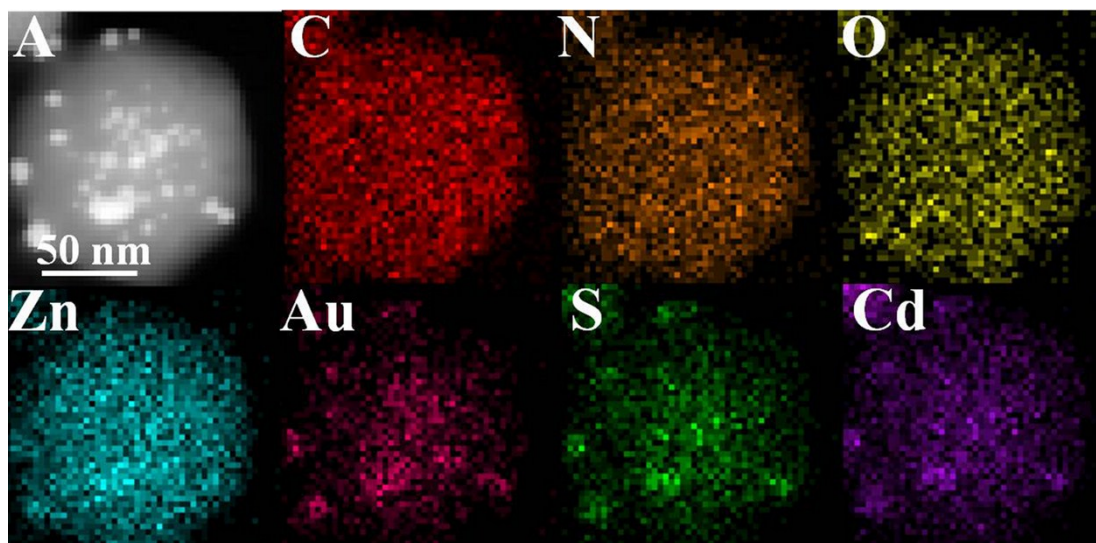


Fig. S4 EDS mapping images of the NPC-ZnO/Au/CdS polyhedra with C, N, O, Zn, Au, S, and Cd.

9. XRD pattern of NPC-ZnO/Au/CdS polyhedra

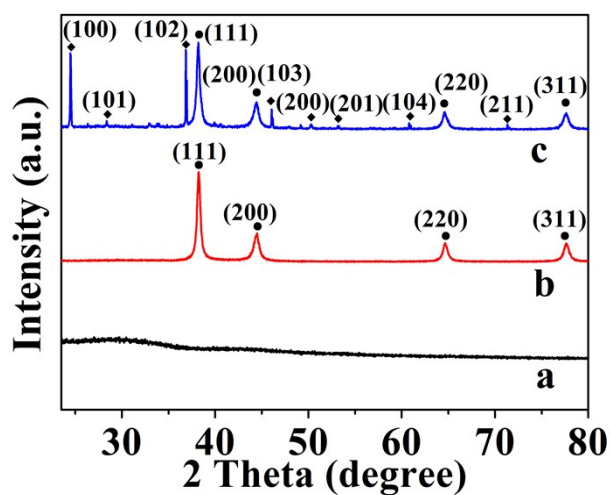


Fig. S5 XRD pattern of NPC-ZnO/Au/CdS polyhedra.

10. XPS spectrum of NPC-ZnO/Au/CdS polyhedra

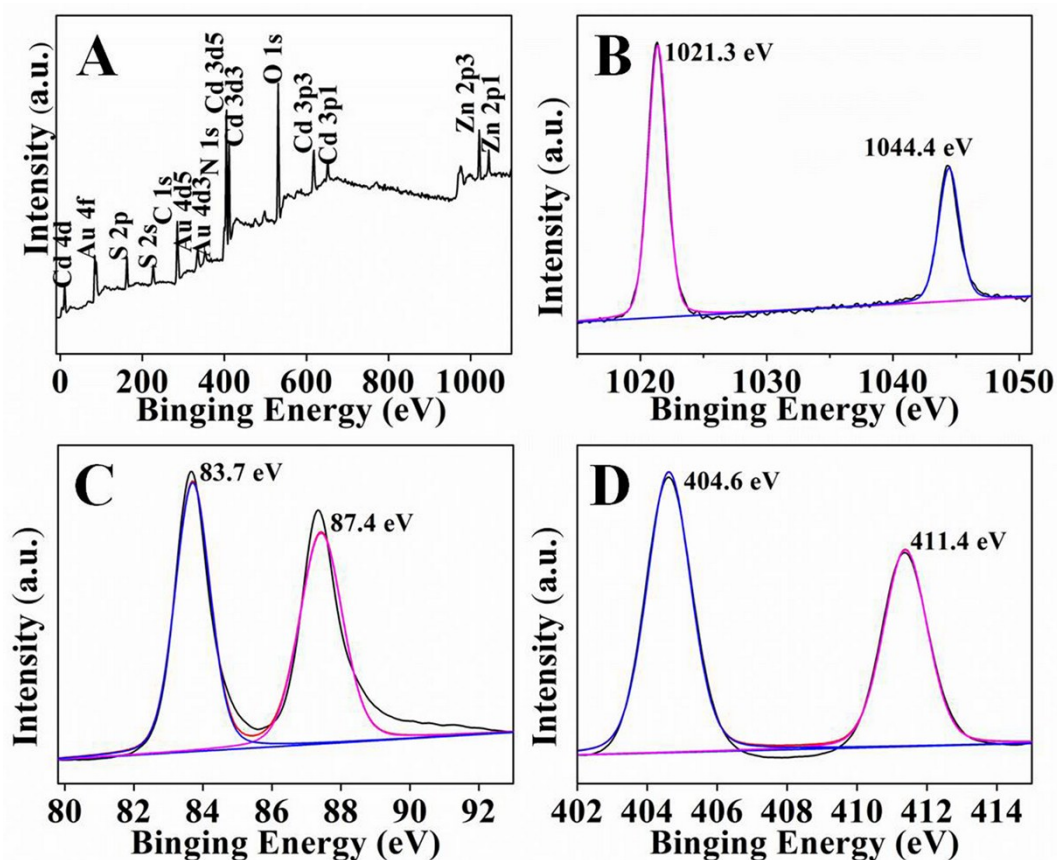
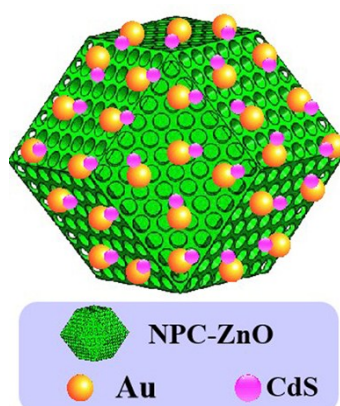


Fig. S6 XPS spectrum (A) of NPC-ZnO/Au/CdS polyhedra and High-resolution spectra of Zn 2p (B), Au 4f (C) and Cd 3d (D).

11. The schematic illustration of the structure of this NPC-ZnO/Au/CdS polyhedra



Scheme S1 The schematic illustration of the structure of this NPC-ZnO/Au/CdS polyhedra.

12. The possible electron-transfer mechanisms of ITO/NPC-ZnO/Au and ITO/NPC-ZnO/Au/CdS electrodes

In order to explore the possible electron-transfer mechanisms of ITO/NPC-ZnO/Au and ITO/NPC-ZnO/Au/CdS electrodes, the conduction band (CB) and the valence band (VB) of NPC-ZnO and CdS were investigated by electrochemical method (Fig. S7) [2, 3]. The results show that NPC-ZnO has a CB edge at -0.89 V and a VB edge at 1.73 V, and CdS has a CB edge at -1.01 V and a VB edge at 1.08 V vs. saturated calomel electrode (SCE). That is, the CB and VB potentials of NPC-ZnO are -0.65 and 1.97 V, and those of CdS are -0.77 and 1.32 V vs. the normal hydrogen electrode (NHE), respectively.

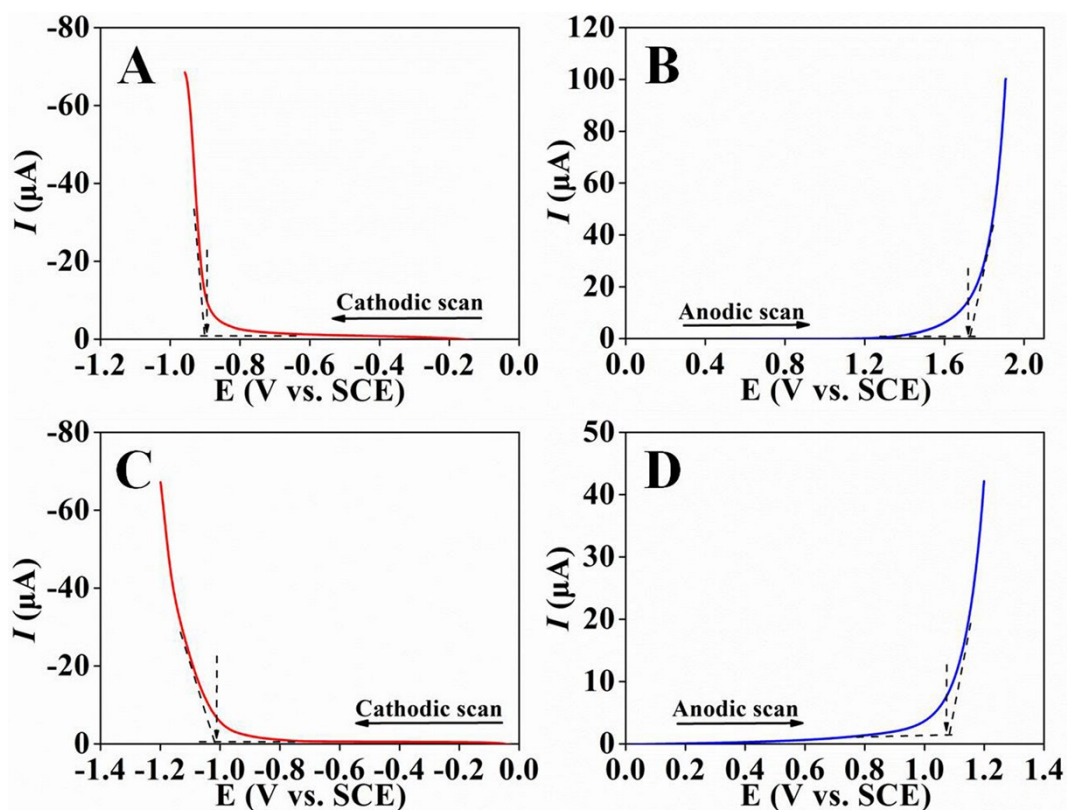
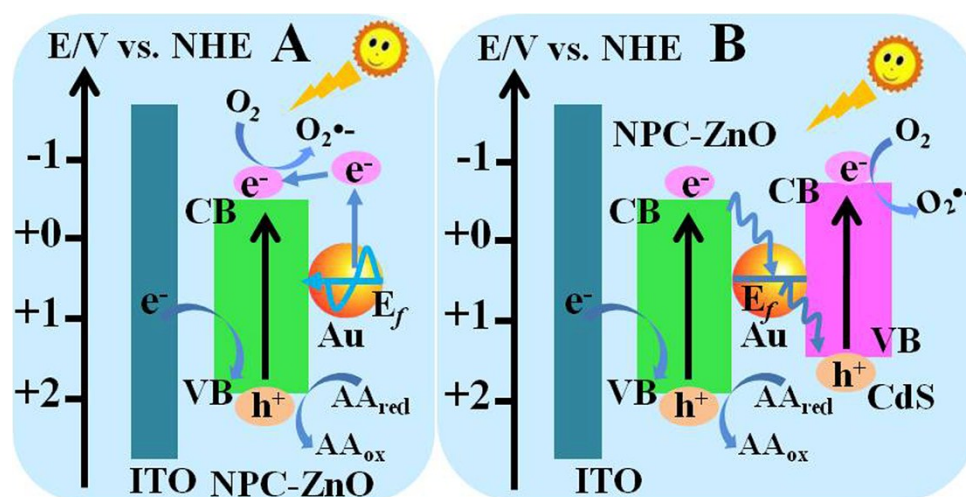


Fig. S7 Cathodic and anodic linear potential scans for determining the conduction (CB) and valence band edge (VB) of NPC-ZnO polyhedra (A, B) and CdS (C, D) in N_2 -saturated Tris-HCl solution (0.1 M, pH 7.4).

Based on the results shown in Fig. S7, the possible electron-transfer mechanisms of the ITO/NPC-ZnO/Au and ITO/NPC-ZnO/Au/CdS electrodes (Scheme S2) are as follows: in case of ITO/NPC-ZnO/Au (Scheme S2A), the surface Plasmon decay generates electron-hole pairs within the Au NPs based on the strong SPR effect of Au NPs (one of the most important characteristics of Au NPs) [4]. The potential value of the generated hot electrons of Au NPs is more negative than the value of the conduction band (CB) of NPC-ZnO [4-7]. This results in the injection of the generated hot electrons of Au NPs into the CB of NPC-ZnO and an enhanced

photocurrent can be observed. For the NPC-ZnO/Au/CdS (Scheme S2B), a “Z”-type migration pathway of electrons is formed. The photo-generated electrons on the CB of NPC-ZnO (-0.65 V vs NHE) transfer to the VB (1.32 V vs NHE) of CdS via an electron mediator (a conductor, such as Au, Ag, Pt, Pd, or reduced graphene oxide [8]. In this work, we used Au NPs.), and then are further excited to the CB (-0.77 V vs NHE) of CdS for the electrochemical reduction of O₂ (electron acceptors) in the electrolyte [7, 9-11]. Meanwhile, AA can effectively be oxidized by photo-generated holes to reduce the recombination of photo-generated electron-hole pairs. Thus, a large cathodic photocurrent is obtained.



Scheme. S2 The possible electron-transfer mechanisms of (A) ITO/NPC-ZnO/Au and (B) ITO/NPC-ZnO/Au/CdS electrodes. E_f , Fermi level.

13. Hemin-induced photocurrent-polarity switching

To investigate the hemin-induced photocurrent-polarity switching of the ITO/NPC-ZnO/Au/CdS electrode, several control experiments were carried out (Fig. S8). It is noted that the ITO/hemin electrode generates a very small cathodic

photocurrent (curve a, $-5.085 \times 10^{-3} \mu\text{A}$). And the enhanced cathodic photocurrents are obtained for the ITO/NPC-ZnO/hemin electrode ($-1.855 \mu\text{A}$, curve b), ITO/NPC-ZnO/Au/hemin electrode ($-3.152 \mu\text{A}$, curve c) and ITO/NPC-ZnO/Au/CdS electrode ($-4.047 \mu\text{A}$, curve d), respectively. However, when the ITO/NPC-ZnO/Au/CdS electrode is modified with hemin, the photocurrent polarity of the electrode is changed from the cathodic photocurrent (curve d) to anodic photocurrent (curve e) and a large anodic current is observed ($15.528 \mu\text{A}$, curves e). This indicates clearly the hemin-induced photocurrent-polarity switching of the ITO/NPC-ZnO/Au/CdS electrode.

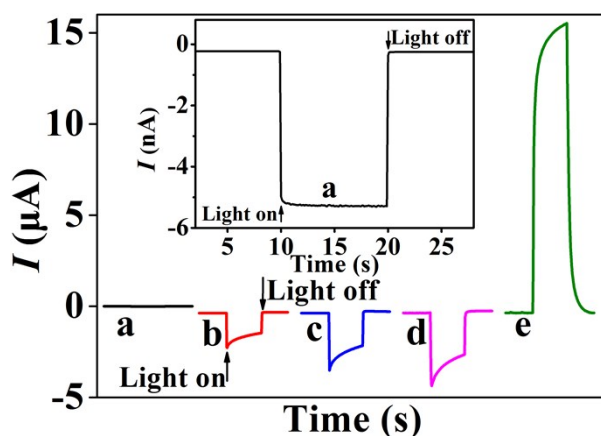


Fig. S8 Photocurrent responses of (a) ITO/hemin, (b) ITO/NPC-ZnO/hemin, (c) ITO/NPC-ZnO/Au/hemin, (d) ITO/NPC-ZnO/Au/CdS and (e) ITO/NPC-ZnO/Au/CdS/hemin electrodes in 0.1 M Tris-HCl (pH 7.4) containing 0.1 M AA at -0.3 V under visible light illumination ($\lambda > 420 \text{ nm}$). hemin (20 μL , 0.1 mM).

In order to clarify the influence of the hemin concentration on the PEC performance of the ITO/NPC-ZnO/Au/CdS electrode, another control experiment was

carried out and the corresponding results are shown in Fig. S9. As shown in Fig. S9, when the concentration of hemin is quite low, the cathodic photocurrent of the ITO/NPC-ZnO/Au/CdS/hemin electrode increases with the increase of hemin concentration, due to that the NPC-ZnO/Au/CdS electrode is sensitized by hemin [12]. When the concentration of hemin is further increased, both cathodic and anodic photocurrents are observed during the light-on process (curves d and e). The high concentration of hemin results in that only anodic photocurrent can be observed and the anodic photocurrent increases with the increase of the hemin concentration (curves f, g and h). This implies that the photo-generated electrons transfer to the ITO electrode with the simultaneous transfer of electrons from hemin to CdS.

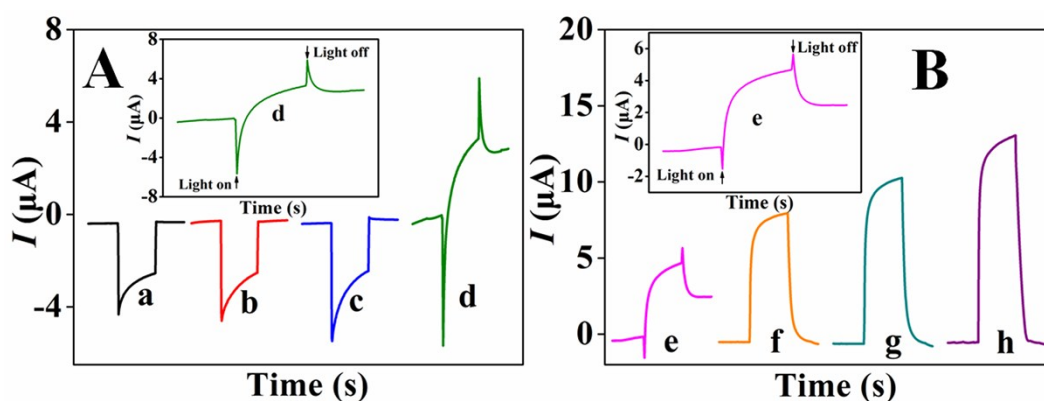
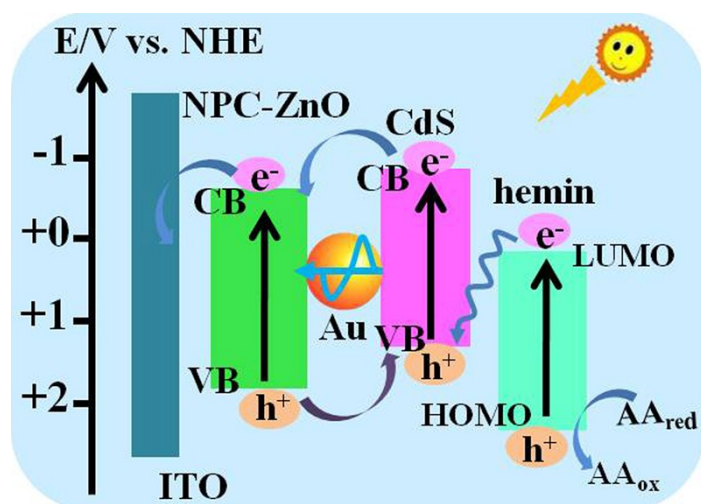


Fig. S9 Effect of hemin concentration on the photocurrent response of the ITO/NPC-ZnO/Au/CdS/hemin electrode in 0.1 M Tris-HCl (pH 7.4) containing 0.1 M AA at -0.3 V under visible light illumination ($\lambda > 420 \text{ nm}$). The volume of hemin solution, 20 μL ; hemin concentration: (a) 0, (b) 0.1 nM, (c) 1 nM, (d) 8 nM, (e) 10 nM, (f) 50 nM, (g) 200 nM, and (h) 1000 nM.

Based on the hemin-induced photocurrent-polarity switching and large amounts of hemin/G-quadruplex generated by HCR amplification strategy, a new assay strategy has been developed (Scheme 1). According to the results shown in Fig. S7-S9, the possible photocurrent generation mechanism of the developed PEC sensing platform is as follows (Scheme S3): under visible light excitation, the electrons of hemin are excited from its highest occupied molecular orbital (HOMO, 2.46 V vs NHE) to lowest unoccupied molecular orbital (LUMO, 0.18 V vs NHE), and further transfer from the LUMO of hemin to the VB (1.32 V vs NHE) of CdS due to the matched energy level between hemin and CdS [12]. Then, the electrons on the CB of CdS (-0.77 V vs NHE) transfer to the CB of NPC-ZnO (-0.65 V vs NHE). Here, Au NPs between NPC-ZnO and CdS not only act as a mediator to enhance the electron transfer, but also serve as an energy conveyor to transfer the energy from CdS to NPC-ZnO [13]. Thus, the efficient separation of electron-hole pairs is achieved and a large anodic photocurrent is generated.



Scheme. S3 The possible photocurrent generation mechanism of the developed PEC sensing platform.

14. Optimization of experimental conditions

To achieve the excellent performance of the developed biosensor for TB detection, several experimental parameters, including TBA1 concentration, TB incubation time, and the incubation time of HP1+HP2+hemin were optimized.

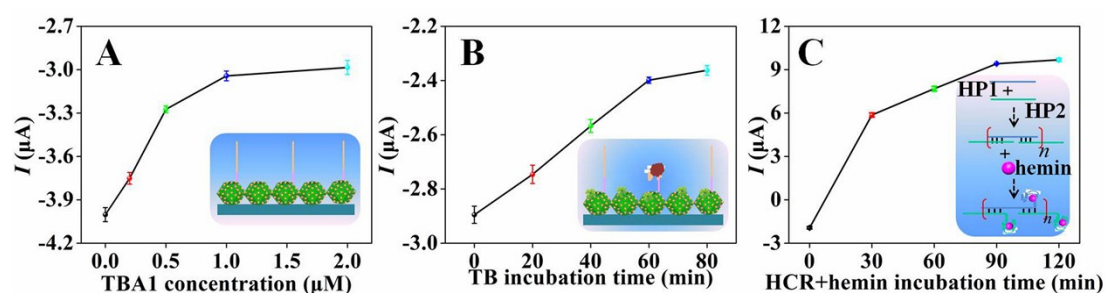


Fig. S10 Effects of some parameters on the photocurrents of the modified electrodes.

(A) The concentration of TBA1; (B) the incubation time of TB (TBA1 concentration, 1 μM ; TB concentration, 20 pM); (C) the incubation time of HP1+HP2+hemin (TBA1 concentration, 1 μM ; TB concentration, 20 pM ; TB incubation time, 60 min).

The influence of TBA1 concentration on the photocurrent of the ITO/NPC-ZnO/Au/CdS/TBA1 electrode was analyzed. With the increase of TBA1 concentration, the cathodic photocurrent decreases due to the blocking effect of the poor-conductive TBA1. From Fig. S10A, a plateau is reached at 1 μM . Thus, 1 μM is chosen as the optimal TBA1 concentration.

The incubation time of TB is a key parameter and also optimized. Fig. S10B shows that the longer incubation time is, more TB molecules are introduced to the sensing system, resulting in a decreased cathodic photocurrent. After 60 min, the cathodic photocurrent reaches a plateau. Thus, 60 min is employed for the TB incubation time in this work.

In addition, the incubation time of HP1+HP2+hemin affects the amount of HP1+HP2 duplex on the surface of the modified electrode, and indirectly affects hemin amount. Therefore, the optimal incubation time of HP1+HP2+hemin is evaluated. As shown in Fig. S10C, the anodic photocurrent increases with the increase of incubation time and a plateau can be obtained at 90 min. Thus, 90 min is chosen as the optimal incubation time of HP1+HP2+hemin.

15. Comparison of various PEC methods for TB assay

Table S1. Comparison of various PEC methods for TB assay

| Strategy | Linear range (pM) | LOD (fM) | IS (μA pM^{-1}) ^a | Ref. |
|--|----------------------|-------------|---|------|
| pH meter readouts | 0.1–1000 | 50 | 10 | [14] |
| G-quadruplex/hemin switched-on photocurrent of PbS | 0.1–10000 | 15 | 0.04 | [15] |
| Au and Exo III-assisted signal amplification | 0.02–10 | 9.6 | 0.6 | [16] |
| DNA–protein interaction | 10–10260 | 1000 | 0.05 | [17] |
| graphene and CdSe multilayers | 1–10 | 450 | 0.012 | [18] |
| CeO ₂ and PTNs-electron transfer tunneling distance regulation | 0.02–100 | 6.7 | 1500 | [19] |
| Ag/TiO ₂ /3D nitrogen doped graphene hydrogel | 0.01–10 | 3 | 50 | [20] |

| | | | | |
|--|--------------|-------|-------|-----------|
| MnPP//PTCA | 0.01–10000 | 3 | 250 | [21] |
| AuNPs//CdS energy-transfer | 0.001–10 | 0.1 | 4000 | [22] |
| energy-transfer CdS and Au | 0.003–513 | 1.3 | 1167 | [23] |
| Target-induced photocurrent-polarity switching | 0.0008–0.015 | 0.089 | 72783 | This work |

^aIS (Initial sensitivity) = $(I_1 - I_0)/C_1$, where I_0 is photocurrent of the sensor incubated without TB, and I_1 is photocurrent of the sensor incubated with TB at the lower response limit of its concentration (C_1).

The reasons about the high sensitivity of the developed PEC sensor may be as follows: (1) the ITO/NPC-ZnO/Au/CdS electrode has a large cathodic background photocurrent due to the indirect Z-scheme NPC-ZnO/Au/CdS system; (2) target-induced switching from indirect Z-scheme NPC-ZnO/Au/CdS to direct Z-scheme CdS/hemin systems results in the high-efficiency photocurrent polarity switching; (3) large amounts of hemin/G-quadruplex generated by HCR amplification strategy further enhance the switch effect of hemin. These lead to the change of the photocurrent of the electrode from cathodic to anodic currents even at very low concentration of TB.

16. Selectivity, reproducibility and stability

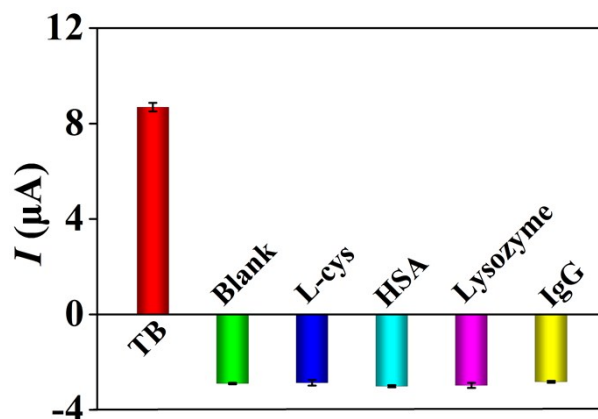


Fig. S11 Selectivity of the developed PEC biosensor. The TB concentration, 10 pM; the concentrations of other proteins (L-cys, HSA, lysozyme and IgG), 500 pM.

To evaluate the reproducibility of the developed PEC biosensor for TB assay, five electrodes prepared separately in the same conditions were used to detect TB (10 pM), and the relative standard deviation (RSD) is 2.1%. In addition, the stability of the PEC biosensing system was further investigated by storing them at 4 °C in refrigerator. The photocurrent of the biosensor can maintain about 96.3% of its initial photocurrent after 2 weeks. These results demonstrate the good reproducibility and satisfactory stability of the prepared PEC biosensor.

17. Recovery test

To investigate the analytical applicability of the proposed PEC biosensing platform in complex biological system, various concentrations of TB (1.0, 5.0, 10, and 15 fM) were added in the 10-fold diluted (10 mM PBS, pH 7.4) human serum samples, and the recoveries were evaluated and are 99%, 104%, 96%, and 107%,

respectively (Table S2). The results indicate that the developed PEC biosensor has potential applications in target assay in actual samples.

Table S2. Recovery tests of TB in the human serum samples.

| Sample | Added (fM) | Found (fM) | RSD (%) | Recovery (%) |
|--------|------------|------------|---------|--------------|
| 1 | 1.0 | 0.99 | 2.6 | 99 |
| 2 | 5.0 | 5.2 | 3.9 | 104 |
| 3 | 10 | 9.6 | 5.2 | 96 |
| 4 | 15 | 16 | 6.3 | 107 |

18. References

- [1] R. Y. Yang, X. X. Yan, Y. M. Li, X. H. Zhang and J. H. Chen, *ACS Appl. Mater. Interfaces* 2017, **9**, 42482–42491.
- [2] G. L. Wang, J. X. Shu, Y. M. Dong, X. M. Wu, W. W. Zhao, J. J. Xu and H. Y. Chen, *Anal. Chem.* 2015, **87**, 2892–2900.
- [3] T. F. Yeh, S. J. Chen, C. S. Yeh and H. Teng, *J. Phys. Chem. C.* 2013, **117**, 6516–6524.
- [4] J. Shu, Z. L. Qiu, S. Z. Lv, K. Y. Zhang and D. P. Tang, *Anal. Chem.* 2018, **90**, 2425–2429
- [5] H. Li, F. Qin, Z. Yang, X. Cui, J. Wang and L. Zhang, *J. Am. Chem. Soc.* 2017, **139**, 3513–3521.
- [6] R. y. Li, R. Yan, J. C. Bao, W. W. Tu and Z. H. Dai, *Chem. Commun.* 2016, **52**, 11799–11802.

- [7] R. J. Zeng, Z. B. Luo, L. S. Su, L. J. Zhang, D. P. Tang, R. Niessner and D. Knopp, *Anal. Chem.* 2019, **91**, 2447–2454.
- [8] J. Low, J. Yu, M. Jaroniec, S. Wageh and A. Al-Ghamdi, *Adv. Mater.* 2017, **29**, 1601694.
- [9] H. Tada, T. Mitsui, T. Kiyonaga, T. Akita and K. Tanaka, *Nat. Mater.*, 2006, **5**, 782–786.
- [10] L. Q. Ye, J. Y. Liu, C. Q. Gong, L. H. Tian, T. Y. Peng and L. Zan, *ACS Catal.* 2012, **2**, 1677–1683.
- [11] S. Y. Wang, Y. Y. Gao, Y. Qi, A. L. Li, F. T. Fan and C. Li, *J. Catal.* 2017, **354**, 250–257.
- [12] G. L. Wang, T. T. Gu, Y. M. Dong, X. M. Wu and Z. J. Li, *Electrochem. Commun.* 2015, **61**, 117–120.
- [13] Z. B. Luo, L. J. Zhang, R. J. Zeng, L. S. Su and D. P. Tang, *Anal. Chem.* 2018, **90**, 9568–9575.
- [14] J. Wang, M. M. Song, C. G. Hu and K. B. Wu, *Anal. Chem.* 2018, **90**, 9366–9373.
- [15] G. L. Wang, J. X. Shu, Y. M. Dong, X. M. Wu, W. W. Zhao, J. J. Xu and H. Y. Chen, *Anal. Chem.* 2015, **87**, 2892–2900
- [16] C. X. Li, W. S. Lu, M. Zhu and B. Tang, *Anal. Chem.* 2017, **89**, 11098–11106.
- [17] Z. Y. Ma, Y. F. Ruan, N. Zhang, W. W. Zhao, J. J. Xu and H. Y. Chen, *Chem. Commun.* 2015, **51**, 8381–8384.
- [18] X. R. Zhang, S. G. Li, X. Jin, S. S. Zhang, *Chem. Commun.* 2011, **47**, 4929–4931.
- [19] J. Xue, L. N. Zhang, C. M. Gao, P. H. Zhu and J. H. Yu, *Biosens. Bioelectron.* 2019, **133**, 1–7.
- [20] N. Hao, R. Hua, S. B. Chen, Y. Zhang, Z. Zhou, J. Qian, Q. Liu and K. Wang,

Biosens. Bioelectron. 2018, **101**, 14–20.

[21] L. J. Huang, L. Zhang, L. Yang, R. Yuan and Y. L. Yuan, *Biosens. Bioelectron.* 2018, **104**, 21–26.

[22] F. Xu, Y. C. Zhu, Z. Y. Ma, W. W. Zhao, J. J. Xu and H. Y. Chen, *Chem. Commun.* 2016, **52**, 3034–3037.

[23] Z. Y. Ma, Y. F. Ruan, F. Xu, W. W. Zhao, J. J. Xu and H. Y. Chen, *Anal. Chem.* 2016, **88**, 3864–3871.